Broadband Miniaturized UWB Antenna for GPR, Wireless Communication, and Radar Systems Spanning Sub-6 GHz, X-, and Ku-Bands

Jinan N. Shehab, Wisam Hayder Mahdi, and Israa Hazem Ali

Original scientific article

***Abstract*—A compact Ultra-WideBand (UWB) microstrip antenna is realized on RT/Duroid 5880 with overall dimensions of 17 × 19 × 0.7 mm³. The slot patch configuration achieves continuous impedance matching from 3.9 to 17.54 GHz, resulting in a −10 dB bandwidth of 13.62 GHz. The three dominant resonant modes are at 3.91 GHz, 10.24 GHz and 16.66 GHz with a strong notch at 9.13 GHz ($|S_{11}| \approx -56$ dB). The realized gain of the antenna from 2.5 to 3.51 dBi across the operating frequency band provides an acceptable performance for use in high-speed, short distance wireless links. Analyses performed in both time and frequency domains have established the UWB properties of the slot patch antenna as demonstrating low group delay variability, well-contained impulse responses and clearly defined eye diagrams. When compared with previously reported designs, the proposed antenna offers a favorable balance between miniaturization, bandwidth, and low-loss performance, making it suitable for UWB, GPR, wireless communication, and radar applications within compact and multi-standard platforms.**

***Index Terms*—Ultra-wideband (UWB), Microstrip antenna, Multi-band operation, Sub-6 GHz communication, X-Band radar, Ku-Band satellite links, Ground-penetrating radar (GPR), Compact design.**

I. Introduction

According to the Federal Communications Commission (FCC), ultra-wideband systems operate above 20% fractional bandwidth or above 500MHz absolute bandwidth [1]. Historically, UWB systems were developed using impulse technology, with very low power spectral density, primarily for military use (radar), secure communications, and underground penetrating radar systems [2]. However, advances in signal processing and regulation approval have allowed for modern UWB systems to also include systems using continuous waveform and modulated transmissions, promoting widespread commercial use of these technologies [3].

UWB provides large amounts of channel capacity, high temporal resolution, and robustness against multipath interference in a variety of applications, including high data-rate short range wireless communication, imaging radar, object detection through walls and medical patient monitoring, etc. [4]. Also, multi-band UWB antennas can cover frequency segments like Sub-6 GHz, X-band, Ku-band, etc., thus enabling a single hardware platform to satisfy many types of heterogeneous must-haves for cutting-edge wireless communications, high-resolution radar, and satellite systems [3], [5]. The ability of multiple UWB antennas to operate in different ways to meet the requirement for small, efficient designs has stimulated a lot of research in the area of UWB antenna miniaturizing while maintaining performance.

Over the last several decades, the design of UWB antennas has changed due to the need for wide impedance bandwidths, equal radiation patterns, and smaller physical size UWB antennas [6]. The early designs of UWB antennas used a combination of planar monopole and planar dipole configurations with their inherent ability to create a wide band of frequencies, as well as easy to manufacture [2]. The downside of most of the earlier designs of UWB antennas was that they required large physical dimensions to create the lower operating frequency, and therefore could not be used in smaller, portable platforms [3].

Various methods have been used by researchers to enhance the anti-jamming characteristics and hence the frequency performance of antennas while also maintaining their performance and without increasing their overall size. Defected Ground Structures (DGS), slot loading, fractal geometries, and parasitic elements are all examples of how to enhance the bandwidth of an antenna while minimizing its size [4], [5]. One of the current areas of interest in the UWB design of antennas is the combination of multi-band capabilities into one single design capable of operating at multiple frequency bands, such as: Sub-6 GHz, X-band Radar and Ku-band satellite links [1]. However, achieving this type of integration while not introducing any unwanted resonances or degrading radiation performance is one of the primary technical obstacles in UWB antenna design [3].

Several UWB antennas have been proposed in many studies as a solution to problems associated with very large ompedance bandwidths, small sizes and suitability for various wireless and radar use cases. These studies used different substrate materials, physical dimensions and operational bandwidths while attempting to optimize their designs to meet application requirements. Examples of these designs include the following:

In [6], authors propose a compact UWB circular patch ante-

Manuscript received December 20, 2025; revised January 19, 2026. Date of publication August 27, 2026. Date of current version August 27, 2026. The associate editor prof. Miroslav Joler has been coordinating the review of this manuscript and approved it for publication.

Authors are with the University of Diyala College of Engineering Ringgold standard institution, Baqubah, Diyala Governorate, Iraq (e-mails: jinan_alazawii_eng@uodiyala.edu.iq, wisam_haider@uodiyala.edu.iq, pg_student75@yahoo.com).

Digital Object Identifier (DOI): 10.24138/jcomss-2025-0207

nna on FR-4 (ε_r= 4.4, 1.6 mm) with overall dimensions of 35 × 35 × 1.6 mm³, offering a −10 dB bandwidth from 11.153 to 14.498 GHz, suitable for high-frequency wireless applications. While in [2], authors present a high-gain compact paddle-shaped UWB antenna on PTFE (ε_r = 2.2, 0.508 mm) with dimensions of 50× 39 mm², operating from 1.9 to 9.2 GHz, intended for ground-penetrating radar and soil inspection applications. In [3], a compact circular fractal UWB antenna on FR-4 (ε_r = 4.4, 1.6 mm) with dimensions of 40 × 24.5 mm², operating from 2.70 to 11.0 GHz with an 8.3 GHz bandwidth, suitable for WLAN, WiMAX, and C/X-band telecommunication applications, has been designed. In [4], a tree-shaped CPW-fed UWB monopole on FR-4 (ε_r= 4.3, 1.6 mm) with dimensions 54 × 36 × 1.6 mm³, using an incomplete ground and a circular patch with two "ears," achieves 1.99–11.56 GHz (≈ 9.6 GHz, 146.7% FBW), 97% radiation efficiency, and ~8 dB peak gain, targeting GPR applications, has been designed. Then in [7], authors present a compact CPW-fed circular microstrip patch antenna on FR-4 ($\varepsilon_r \approx$ 4.4, 1.6 mm) with dimensions 16 × 13 × 1.6 mm³ and radius 5.25 mm operates from 4.0 to 13.19 GHz (9.19 GHz bandwidth), supporting C, WiMAX, WLAN, 4G LTE, 5G midband, V2X, sub-6 GHz, UWB, X, and Ku-band applications. Authors in [1] propose a compact CPW-fed trumpet-shaped planar antenna with symmetrical ground and perturbative slots on FR-4 ($\varepsilon_r \approx$ 4.4, 1.6 mm) with dimensions 168 × 120 × 1.6 mm³ achieves 0.3–18 GHz (≈60:1 ratio), providing omnidirectional coverage across P-, L-, S-, C-, X-, and Ku-bands for wideband spectrum monitoring applications.

There has been progress in UWB antennas but there is still a trade-off between obtaining a wide spectral range by using a smaller element in a more practical substrate. Most designs use large radiative elements or complicated loading methods to achieve a wide bandwidth which makes it difficult to fabricate and integrate these products; whereas smaller antennas can't effectively support Sub-6 GHz, X-Band, and Ku-Band frequencies at the same time and many times will have poor impedance matching. A new continua microminiaturized planar microstrip antenna system was designed that meets these challenges by utilizing an antenna smaller than 20 mm and providing stable multifield characteristics throughout the major frequency ranges.

To overcome this limitation, we present a miniaturized UWB Rogers RT/duroid 5880 (ε_r= 2.2, tanδ = 0.0009, h = 0.7 mm) Micro Strip antenna. The antenna has a footprint of 17 × 19 × 0.7 mm³ and shows resonances at 9.515, 10.235, and 16.675 GHz, while it has a rejection notch at 9.151 GHz ($|S_{11}| \approx -56$ dB). These resonances comprise three contiguous −10 dB bands covering sub-6 GHz, X-band, and Ku-band (3.8–6.7 GHz, 8.6–10.3 GHz, and 15.8–17.7 GHz) all within the same planar structure . The total 3.9–17.5 GHz range of the antenna has been developed without the use of multilayer or 3D loading, and consequently is very easy to manufacture on a printed circuit board and compactly integrated into a small volume.

The major contributions of this research can be summarised as follows:

A miniaturized UWB microstrip antenna with an extremely compact footprint of 17 × 19 × 0.7 mm³ is proposed, achieving wide impedance bandwidth without compromising radiation efficiency.

A stepwise geometric evolution strategy was employed, integrating ground modification, resonant slotting, and parasitic ring loading to establish stable multi-resonant UWB behavior.

The antenna achieves a contiguous −10 dB bandwidth of 3.9–17.54 GHz, simultaneously covering Sub-6 GHz, X-band, and Ku-band, making it suitable for multi-standard wireless and radar systems.

Time-domain performance, including group delay, impulse response, and eye diagram, was evaluated through CST–MATLAB co-simulation, confirming high signal fidelity and suitability for high data-rate UWB links.

According to the comparative findings, the designed antenna is likely to have a good balance of compactness, a large bandwidth and significant gain; this means there will be more efficient use of the size to bandwidth ratio compared to the most recent designs of UWB antennas. The emphasis of this research is towards simulation validation of the design; therefore, further developments are planned to create experimental prototype antennas once the proper fabrication materials and equipment are obtained.

The paper is structured as follows. Section II details the antenna design procedure and its geometric evolution. Section III analyzes the simulated results, focusing on impedance bandwidth, gain behavior, radiation performance, and surface current distribution. System-level performance is then examined in Section IV through S-parameter characterization, group delay, impulse response, eye-diagram analysis, and comparison with recent UWB designs, followed by concluding remarks and application perspectives in Section V.

II. Antenna Design and Configuration

Through a well-structured approach of geometric evolution over the course of seven steps, the proposed antenna emerged as a multifunctional UWB radiator that has been designed in a very compact manner compared to earlier rectangular patch antennas. Each step of the design was implemented using Rogers RT/Duroid 5880 (ε_r= 2.2, tanδ = 0.0009, thickness h = 0.7 mm), which were selected due to their low dielectric loss and broadband stability.

In comparison, the final design combines an overall footprint measuring approximately 17 × 19 × 0.7 mm^3 with feed from a 50-ohm microstrip transmission line. The geometric transformation from traditional rectangular patch antenna to miniaturized compact structure is illustrated in both Figs. 1(a) and 2(a), while simulated reflection coefficient (S_{11}) responses for each step are shown in Figs. 1(b) and 2(b). This development is illustrated through the progression of antenna design phases, demonstrating a consistent incremental improvement on previous designs from design phase to produced structure.

A. Step 1 – Baseline Rectangular Patch

A baseline rectangular microstrip patch was designed on Rogers RT/duroid 5880 with dimensions calculated using the standard patch antenna equations[8]:

$$f_r = \frac{c}{\sqrt{\varepsilon_{eff.} * 4 * L_{eff.}}} \quad (1)$$

where f_r is resonant frequency, c is the speed of light in free space, c is the speed of light in free space, $L_{eff.}$ represented the total effective current path traversed along the horizontal and vertical segments of the stub, while $\varepsilon_{eff.}$ represents the effective permittivity of the guided structure.

To account for the fringing fields that extend beyond the physical boundaries of the microstrip, the effective permittivity is approximated using the well-established relation [8], [9]:

$$\varepsilon_{eff.} = \frac{\varepsilon_r+1}{2} + \frac{\varepsilon_r-1}{2}\sqrt{1+12*\frac{h}{w}}^{\frac{-1}{2}} \quad (2)$$

where ε_r is the relative permittivity of the substrate, h is the substrate thickness, and w is the width of the microstrip line. This exhibited a limited resonant response and a narrow band with poor compatibility at certain frequencies, as illustrated in Fig. 1 (a) and (b) (Step 1).

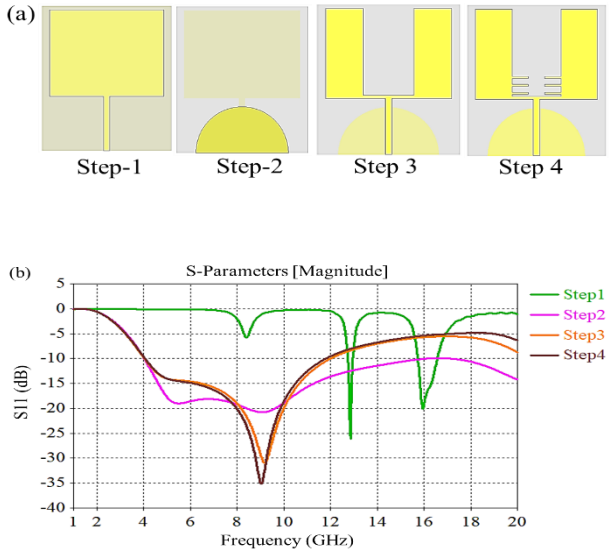


Fig. 1. Geometrical Evolution of the Proposed Antenna (Steps 1–4) and Corresponding Reflection Coefficient (S_{11}) Responses.

B. Step 2 – Ground Modification for UWB Response

A semi-circular plane was substituted for the rectangular ground under the feed to increase surface current traveling distance and improve coupling. The semi-circular shape created a broader impedance bandwidth with first resonance frequency shifted to lower frequencies and provided stable realized gain while retaining the higher order mode near 15-16 GHz. This step represented the first step towards achieving an ultra-wideband behaviour when compared to the baseline (Fig. 1(a) and 1(b)).

C. Step 3 – Central Longitudinal Slot

In order to extend the surface current's flow, a vertical slot was cut in the centerline of the patch, therefore extending the current flow without increasing the size of the antenna. The change resulted in a significant decrease in the reflection coefficient S_{11}depth from 8 to 10 GHz, providing improved impedance matching. However, while there was a significant increase in gain stability as shown in Figs. 1(a) and (b) (Step 3), the bandwidth remained relatively narrow with limited extension towards the lower end of the desired response.

D. Step 4 – Symmetric "Teeth" Extensions

Two symmetric "teeth" stubs have been added to the lower edge of the patch, which act as capacitative reactive elements that enhance the capacitative coupling. This adjustment has enabled improved impedance matching with a significantly larger impedance matching resonance at or around 9 GHz ($|S_{11}|$= -35 dB) and an increased -10 dB gain bandwidth of about 4.069 to 11.79 GHz. The gain response has become more consistent across the entire operating band (Fig. 1(a) and (b); Step 4). To further increase the impedance bandwidth and improve performance, structural changes were made as described in Step 5.

E. Step 5 – Transitional F/E-Shaped Slots in the Patch

On each side of the patch, symmetrical slots F-shaped and E-shaped were etched; this modification extended the path of current [12] and produced three resonant modes with better returns than previous versions although this modification had a minimal effect on broadening the total bandwidth (Fig. 2(a) and (b), Step 5).

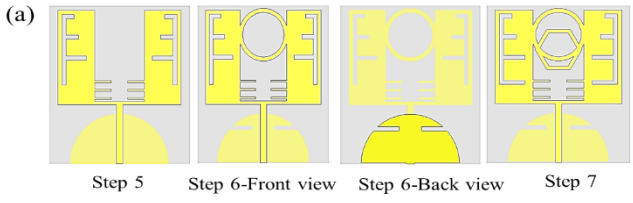
F. Step 6 – Central Parasitic Ring Resonator with Ground Optimization

The parasitic ring in the centre of the patch and use of additional ground improvements were designed to introduced strong resonant coupling and thus, increase both the delivered impedance bandwidth and realised gain as shown in (Fig. 2 (a) and (b) (Step 6).

G. Step 7 – Completed E-slot with Diamond Ring

The final stage of the proposed work involved fully converting the transitional slots into E-slots and creating a concentric ring, in a diamond shape, around the interior of a circular resonator (which significantly improved the symmetry of the current distribution, and Improved the gain and stabilized the impedance matching across UWB frequencies). S_{11} has three distinct resonant modes with increased bandwidth and realized Gain at -10 dB as illustracted in (Fig. 2, Step 7).

The optimized antenna geometry, as illustrated in Fig. 3 and Table I, is fully defined by the dimensional parameters of the radiating patch and the defected ground structure.



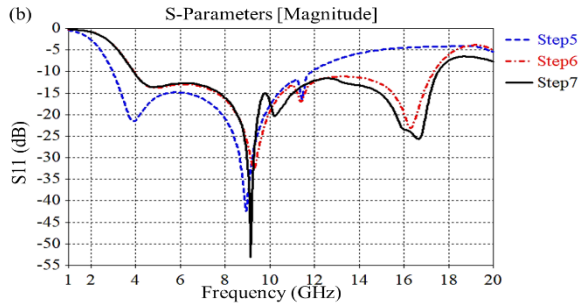


Fig. 2. Advanced Geometrical Evolution of the Proposed Antenna (Steps 5–7) with Corresponding Reflection Coefficient (S_{11}) Characteristics.

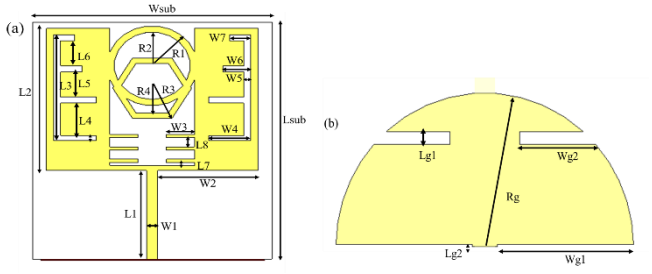


Fig. 3. Geometry and key design parameters of the proposed UWB antenna: (a) front view, (b) back view.

TABLE I
OPTIMIZED GEOMETRICAL PARAMETERS OF THE PROPOSED UWB ANTENNA

Parameter	Description	Dimensions (mm)
Wsub	Width of the substrate	17
Lsub	Length of the substrate	19
hs	Height of substrate	0.7
L1	Length of the feedline	7.1
W1	Width of the feedline	1.2
W2	Half-width of the patch	7.1
L2	Length of the patch	11.4
W3	Width of the teeth in the patch	2
L3	Side line length of the E-slot	8.5
W4	Width of the E-slot1	3
L4	Length of the E-slot1	2.6
L5	Length of the E-slot2	2
L6	Length of the E-slot3	2
W5	Width of the E-slot	0.5
W6	Width of the E-slot2	2
W7	Width of the E-slot3	1.5
Lg1	Length of the slot in the ground	0.5
Wg2	Width of the slot in the ground	3.6
Rg	Semi-circular ground radius	6
R1	Outer circular radius of the patch	3.2
R2	Inner circular radius of the patch	2.7
R3	Inner diamond slot radius	2.8
R4	Outer diamond slot radius	2.3

III. ANTENNA ANALYSIS AND RESULTS

Analysis of the proposed antenna by full-wave simulations regarding reflection coefficient, bandwidth, gain, far field performance was performed. By using the full-wave simulation, all of the successive design revisions were analysed and compared to show the significance of every revision in achieving optimum UWB characteristics with stable gain characteristics.

A. Reflection Coefficient (S_{11})

The reflection coefficient of the proposed antenna is presented in Fig. 4. The antenna exhibits a broad impedance bandwidth ranging from 3.91 GHz to 17.54 GHz under the –10 dB return loss criterion, corresponding to an absolute bandwidth of 13.62 GHz and a fractional bandwidth (FBW) of approximately 127%, fully satisfying UWB requirements. In this band, three separate resonances were confirmed to provide stable impedance matching throughout the entire bandwidth. A minimum of $|S_{11}| \approx$-53 dB provides excellent return loss and efficient transfer of power from the feed to the radiator. The results demonstrate that all modifications made to the antenna provided improved operational bandwidth while not compromising on performance; demonstrating that this antenna is suitable for UWB use.

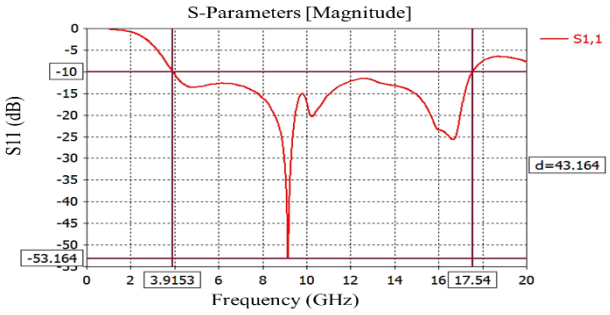


Fig. 4. Simulated reflection coefficient (S11) of the proposed UWB antenna showing the achieved impedance bandwidth (3.91–17.54 GHz).

B. Parametric Analysis of Structural Modifications for UWB Antenna Optimization

A systematic parametric study was performed to assess the influence of key geometrical factors on the impedance response, with all other parameters held constant. The results are summarized in Fig.5 (a–d), where the red curves indicate the optimized values adopted in the final design.

B.1 Effect of Ground Radius (Fig. 5 (a))

The semi-circular ground radius R_g governs the return-current path and the shunt C−L loading seen at the feed, and its influence on bandwidth is optimal at an intermediate value. Both small ($R_g \leq 4$) and large ($R_g \geq 8$) radii degrade, matching and fragment the passband, whereas the mid value R_g=6 (red curve) yields the widest, most continuous −10 dB band (≈ 3.9–17.5 GHz) and preserves the three target resonances. Consequently, R_g = 6 was adopted for the final design.

B.2 Effect of Feed Strip Width (w1, Fig. 5(b))

The feed strip width w_1 primarily controls the input impedance and the balance between inductive and capacitive loading at the feed junction. As observed, narrower strips yield deeper S_{11}notches and a more uniform −10 dB bandwidth, indicating improved impedance matching and reduced return loss. Conversely, wider strips weaken the coupling, leading to shallower resonances and reduced bandwidth continuity. The

optimal value (w ≈0.4) was selected, as it provides the most stable and well-matched response across the UWB band.

B.3 Effect of Central Circular Radius (Fig. 5 (c))

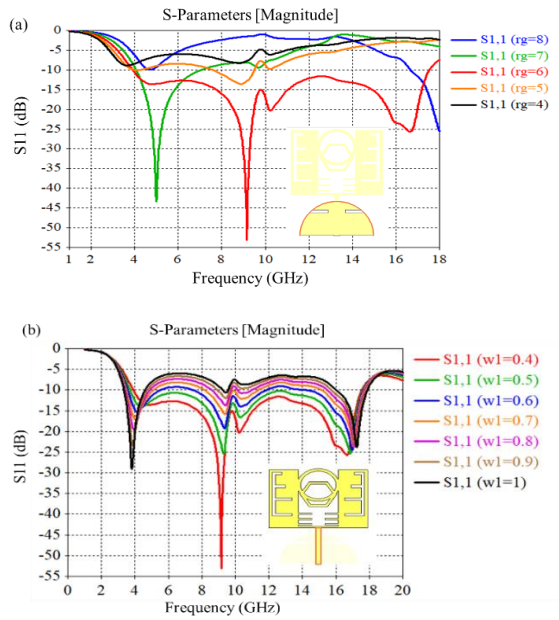
Adjusting the radius of the central circular element influences both the placement of resonant modes and the continuity of the operating band. Larger radii promote wider spectral coverage, whereas smaller values constrain the bandwidth, making the central circle a secondary yet effective parameter for bandwidth tuning.

B.4 Effect of Slot Length (L_3) (Fig. 6d)

L_3 exerts its effect locally at around 10 GHZ, with the shorter the slot length, the deeper resonance depth and, consequently, more effective impedance matching with the longer slot lengths having a reduce the resonance depth. L3 has a very specific response, which can be utilized for accurate control of higher-order resonances.

Collectively, these parameters enable controlled tuning of both global bandwidth behavior and localized impedance matching across the UWB range.

Although experimental fabrication was not conducted, the parametric study gives a practical indication of how the antenna would respond to normal manufacturing tolerances. Real-life PCB manufacturing usually results in small shifts in impedance matching and resonances due to slight dimensional inaccuracies from etching variance or variations in substrate properties, which do not materially disrupt operations over the entire frequency range. The behavior observed in the simulations when varying the feed width, slot length, and ground dimensions is consistent with these expected practical effects. Similarly, small changes in substrate permittivity would mainly result in limited resonance-frequency shifts while preserving the overall UWB performance. This similarity between the simulated parametric behavior and the variations commonly introduced during fabrication suggests that the proposed design can tolerate typical manufacturing and material deviations.



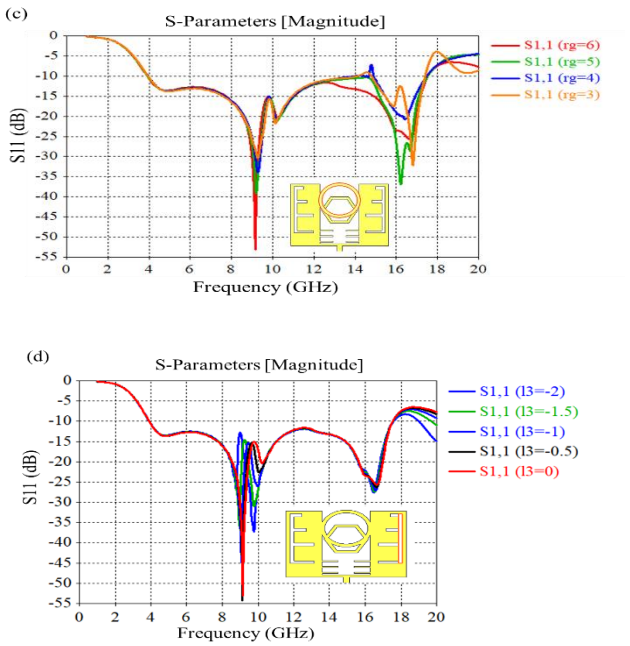


Fig. 5. Parametric study of the proposed UWB antenna:(a) Effect of ground radius (Rg) variation. (b) Effect of feedline width (W_1). (c) Central circular radius (Rg).(d) Effect of slot length (L_3).

C. Comprehensive Radiation Performance Analysis

Aspects of the radiation behavior of the antenna performance are: realised gain; Directivity; efficiency; Voltage Standing Wave Ratio (VSWR); and other key metrics [4], [5], [7], [13]. all this parameters were measured at the three dominant resonant frequencies (9.15, 10.234, and 16.675 GHz) and these values are shown in Table II and subsequently presented in Figs 6 and 7, and thus these values can be used to validate the broadband capabilities of the antenna, and the electromagnetic performance of the antenna across all operational frequencies from 3.9 to 17.6 GHz.

In terms of radiation performance, the realized gain exhibits a quasi-linear increase with frequency, ranging from ~2.5 dBi at 9.15 GHz to ~3.5 dBi at 16.68 GHz, as shown in Table II and Figs 6 and 7 (a). Such behavior is particularly significant since maintaining a steadily rising gain over a wideband antenna is non-trivial; it highlights the effectiveness of the adopted radiating geometry in controlling current distribution and mitigating surface-wave losses [3], [4], [5]. Parallel to this, the directivity also improves with frequency, reaching ~5 dBi at the upper band edge as shown in Fig. 6 (d), which corresponds to more confined and directional radiation patterns, as observed in the 3D plots. Near the lower band edge (~4 GHz) in Fig. 7(a), the realized gain dips to −1 dBi due to edge-of-band excitation and efficiency losses in the miniaturized structure. Across the effective operating band (≈3.9–17.6 GHz), however, the gain remains stable within 2.5–3.5 dBi, ensuring reliable performance for UWB, GPR, and radar applications.

A consistent VSWR < 2 across the full bandwidth confirms excellent impedance matching and minimal return loss, as shown in Figure 7 (b), with the lowest recorded value approaching 1.0, which reflects nearly ideal conditions [13]. This ensures efficient transmission and validates the structural

tuning of the antenna.

The efficiency analysis reinforces the strength of the design. The antenna operates across a broad frequency range and has a radiation efficiency that ranges from 70% to 80%; these efficiencies are an excellent results for compact UWB antennas. The efficiencies of approximately 78% at 9.15 GHz, ~79% at 10.23 GHz, and ~71% at 16.68 GHz indicate excellent energy transfer with minimal dielectric and ohmic losses as shown in Table II and Fig. 6.

The combined results confirm that the proposed antenna provides wideband impedance matching while offering suitable gain, high directional performance, and very good efficiency throughout the frequency range of 3.9 to 17.6 GHz. The quasi-linear gain progression, stable VSWR values, and sustained efficiency illustrate that the design is reliable and suitable for use in UWB and future wireless communication systems, as well as for other modern wireless applications, such as: Sub-6 GHz 5G, Wi-Fi (IEEE 802.11 a/n/ac), WiMAX (3.5/5.8 GHz), X-band radar, and Ku-band satellite links. Therefore, this wide coverage provides an excellent foundation for the use of the antenna in multiservice compact communication and sensor platforms.

TABLE II
SIMULATED RADIATION CHARACTERISTICS AND APPLICATION DOMAINS OF THE PROPOSED USWB ANTENNA AT THE THREE DOMINANT RESONANT FREQUENCIES.

Frequency (GHz)	S_{11} (dB)	Realize Gain (dBi)	Directivity (dBi)	Radiation Efficiency (%)	VSWR	Application Domain
9.151	-53.2	2.5	3.6	78	1.0044	covering UWB indoor communications (3.9–10.6 GHz, partial FCC band), C-band & WiMAX (3.5/5.8 GHz), Wi-Fi (5 GHz), 5G Sub-6 GHz, X-band radar/sensing (8–12 GHz), Ku-band satellite links (12–18 GHz), with potential use in cognitive radio systems (3–10 GHz), military radar/surveillance (X/Ku bands), and automotive radar-assisted sensing.
10.234	-20.2	2.96	4.07	79	1.2127	
16.675	-25.6	3.51	5.02	71	1.115	

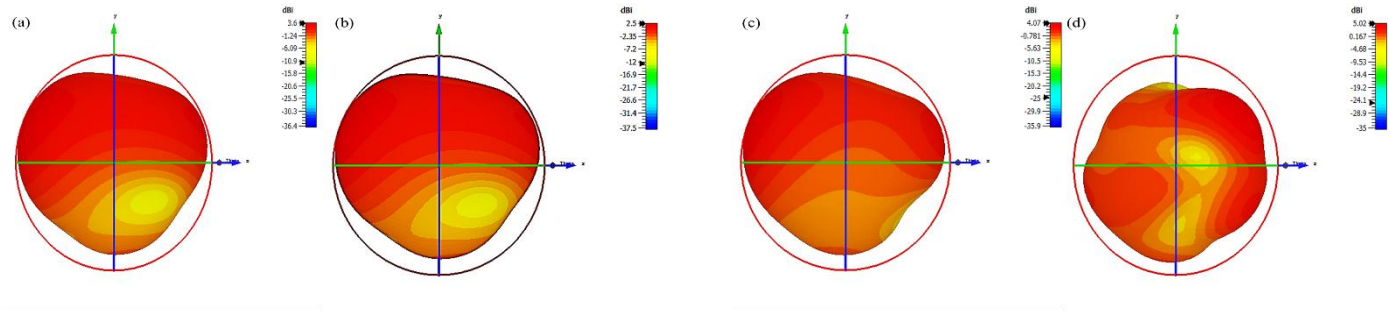


Fig. 6. 3D far-field radiation patterns of the proposed UWB antenna at the main resonant frequencies: (a) Directivity at 9.15 GHz, (b) Realized gain at 9.15 GHz, (c) Directivity at 10.23 GHz, and (d) Directivity at 16.68 GHz.

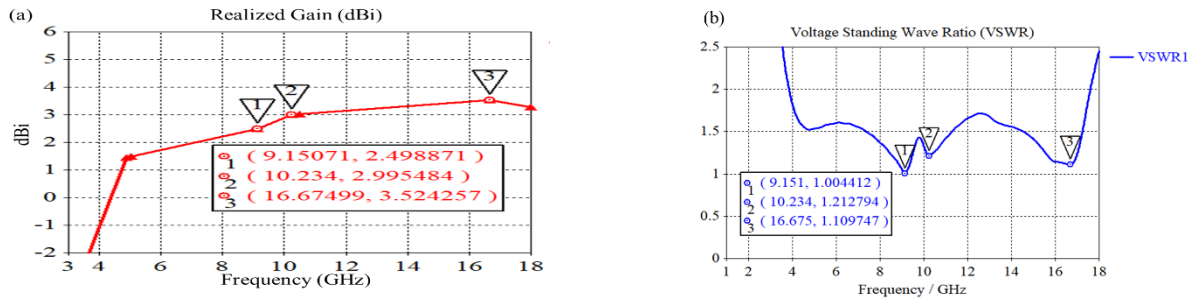


Fig. 7. Simulated radiation performance of the proposed antenna: (a) Realized gain versus frequency, (b) VSWR response across the operating band.

D. Surface Current Distribution

A surface current distribution analysis must be conducted in order to properly assess the performance and efficiency of an antenna, especially in the "critical" low point connecting the feed line and radiating patch. In addition, this data provides insight into the main conduction paths/coupling mechanisms driving the resonant properties and radiation profiles of the proposed design [13], [14].

The surface current distributions at 9.151, 10.234, and 16.675 GHz (Fig. 8 (a–c)) reveal the underlying radiation mechanisms. At 9.15 GHz, strong currents are concentrated along the feedline and ground, confirming effective feed–ground coupling for the fundamental mode.

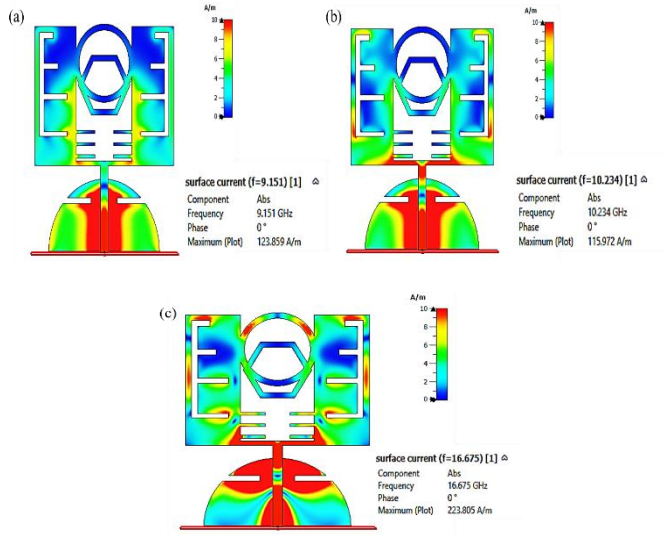


Fig. 8. Simulated surface current distribution of the proposed UWB antenna at the three resonant frequencies: (a) 9.151 GHz, (b) 10.234 GHz, and (c) 16.675 GHz.

At 10.23 GHz, the currents shift toward the side strips and slots, indicating higher-order excitation and improved impedance matching. At 16.67 GHz, multiple current paths become active with strong peaks around the semicircular ground and central slot, enhancing directivity and bandwidth extension. These distributions validate the combined role of the feedline, slots, and ground plane in ensuring stable UWB performance.

E. Mutual Coupling Configuration and Antenna Separation Analysis

To further validate the antenna's suitability for UWB communication, a system-level evaluation was carried out by placing two identical antennas in a face-to-face configuration at different distances (50, 100, and 150 mm). The Transmission Coefficient (S_{21}), group delay, impulse response, and eye diagram were analyzed[3], [15]. This setup does not represent the maximum operational range but rather demonstrates the antenna's ability to maintain stable transmission characteristics over practical link distances. The results confirm low distortion, stable group delay, and a wide-open eye pattern, highlighting the antenna's robustness for high-speed UWB wireless links.

Fig. 9 illustrates the relationship between antenna separation and S_{21}. the antennas exhibit stronger coupling, resulting in higher transmission magnitude but also more interaction effects. As the separation increases to 100 mm, however, the S_{21} level starts to balance out, with less ripple and stable notch frequencies being present; therefore, the optimum coupling vs. isolation is represented here. As antenna separation increases to 150 mm and beyond, the coupling becomes weaker, and that is reflected in the drop off S_{21}levels and lower efficiency of transmission, which supports previously published results on antenna theory [8], [16].

This behavior confirms that moderate separation (around 100 mm) provides the best compromise for UWB operation, ensuring efficient power transfer, minimized distortion, and stable temporal characteristics, while both shorter and longer distances degrade the transmission quality.

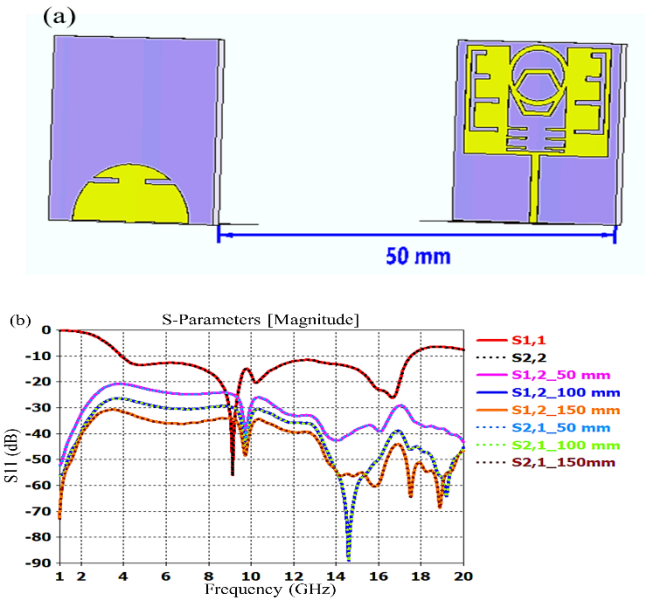


Fig. 9. Simulated mutual coupling analysis of two identical antennas in a face-to-face configuration: (a) antenna arrangement with varying separation distances, and (b) corresponding S-parameters (S_{11}, S_{21}) for separations of 50, 100, and 150 mm.).

F. Time-Domain and Link-Quality Evaluation (MATLAB)

To further verify the antenna's capability for UWB applications, a system-level analysis was conducted at the optimal antenna separation of 100 mm. The evaluation included the S_{21}, group delay, impulse response, and eye diagram.

F.1 Transmission Coefficient (S_{21}) (Fig. 10 (a))

The $|S_{21}|$ reflects the efficiency of power transfer between the antennas. Higher values indicate lower loss and stronger coupling, while reduced levels imply weaker transfer [17]. The $|S_{21}|$ results demonstrate stable transmission with relatively low attenuation across the UWB spectrum, with only minor variations near the resonant notches. This confirms efficient energy transfer between antennas.

F.2 Group Delay (Fig. 10 (b))

Group delay reflects how uniformly signal components arrive across the band. A nearly constant response implies low distortion and dependable wideband transmission [3], [15]. In this design, the group delay stays close to 0 ns. Only minor variations appear near the resonant points. This indicates very limited temporal dispersion and negligible Inter-Symbol Interference (ISI).

F.3 Impulse Response (Fig. 10. c) and d))

The impulse response shows how the antenna reacts to a very short excitation pulse. A narrow, well-defined response suggests that the signal is preserved with little temporal spreading, which is important for UWB operation [3], [15]. In

this case, a distinct pulse appears at about 0.02 ns and quickly fades. This behavior confirms that the antenna maintains time-domain accuracy and can transmit UWB pulses without noticeable distortion.

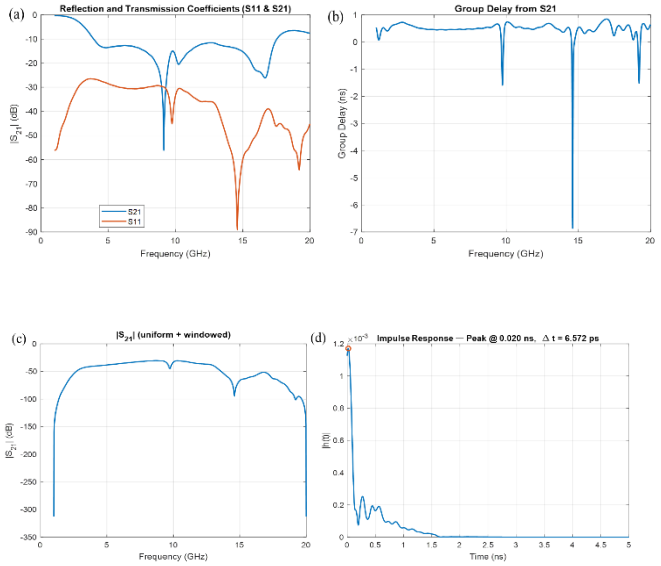


Fig. 10. Time-domain and link-quality evaluation of the proposed UWB antenna at 100 mm separation, including (a) reflection coefficient (S_{11}) and transmission coefficient (S_{21}), (b) group delay, (c) transmission magnitude response, and (d) impulse response.

F.4 Transmit and Filtered Signals (Fig. 11. (a) and (b))

Transmit–filtered analysis illustrates how the antenna channel affects a Non-Return-to-Zero (NRZ) pulse [18]. The filtered waveform exhibits minor temporal spreading but retains its overall shape and polarity, confirming minimal distortion and reliable symbol transmission for UWB links.

F.5 Eye Diagram (Fig. 11. (c))

An Eye Diagram provides a visual indication of the quality of links at high data rates (10 Gb/s) and whether symbols can be clearly distinguished (open eye) or whether symbols are distorted due to noise or interference (closed eye) [19]. In this design at 10 Gb/s, the Eye Diagram has a wide-open eye and has clear symbol separation, indicating high signal integrity and robustness to demanding data-rate conditions. The slight amount of jitter measured is common at these rates and does not affect reliable decoding and therefore validate the suitability of the antenna used for high-speed UWB communication.

F.6 Port Time-Domain Signals (Figure 11. (d))

Port signals demonstrate that the antenna system has properly received input pulse signals indicating high transmission fidelity from the properly aligned output ports [3]. The results presented here indicate the transmitted pulse signals maintain their good sharpness and have very little distortion through any of the ports ($o_{1,1}$ to $o_{2,2}$) indicating that UWB performance is reliable.

In conclusion, the MATLAB validation confirms that the proposed antenna has low distortion and stable time characteristics and can be reliably used for high-speed UWB wireless connectivity. Although the design can be made in accordance with manufacturing tolerances, it was not pursued as due to manufacturing limitations at the Rogers RT/duroid 5880 substrate (0.7 mm thick). therewith, the combination of simulation and systems testing provides sufficient confidence in the antennas' ability to support UWB applications..

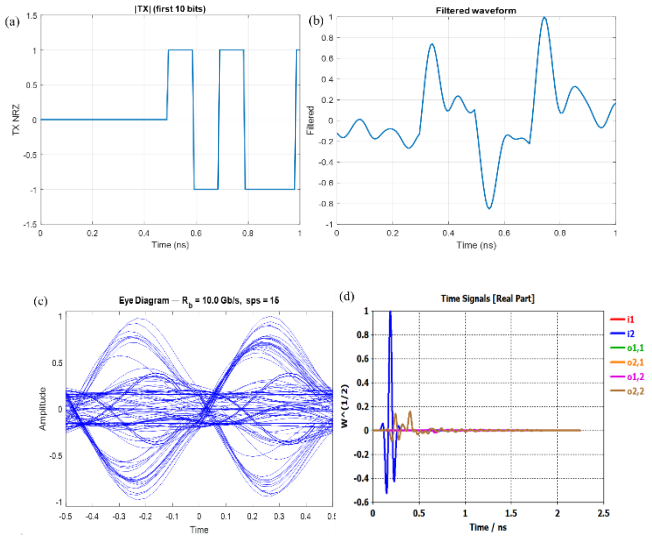


Fig. 11. Time-domain and link-quality evaluation at 100 mm antenna separation: (a) transmitted NRZ pulse, (b) filtered signal, (c) eye diagram at 10 Gb/s, and (d) time signals at different ports.

IV. Comparative Performance Evaluation

The increasing demand for compact and broadband antennas in modern UWB applications, such as radar, high-speed WLAN, and 5G Sub-6 GHz services, has motivated extensive research into designs that can achieve wide impedance bandwidth, good gain progression, and stable radiation performance within a minimal footprint. To address these requirements, the proposed antenna introduces a stepwise structural refinement, combining ground modifications, etched slots, and resonant loops, that effectively broadens the impedance bandwidth (3.9–17.6 GHz) while maintaining high radiation efficiency.

Unlike several reported UWB antennas that either suffer from limited bandwidth or require large physical dimensions, the proposed design achieves wideband coverage, stable VSWR (<2), and linearly increasing gain, all within a compact structure built on a 0.7 mm substrate. This balance ensures suitability for multi-standard applications spanning C-band, X-band, and Ku-band, as well as emerging high-speed wireless platforms.

Table III provides a comparative summary of the proposed antenna against recent state-of-the-art UWB designs. The comparison considers key performance metrics such as bandwidth, resonant frequencies, realized gain, and occupied size. The results demonstrate that the proposed antenna offers a superior trade-off between compactness, wideband impedance matching, and consistent radiation performance, making it a strong candidate for next-generation UWB and multi-standard communication systems.

TABLE III
PERFORMANCE COMPARISON BETWEEN THE PROPOSED ANTENNA AND EXISTING UWB DESIGNS IN TERMS OF SIZE, OPERATING BANDWIDTH AND GAIN.

Ref.	Dim. (mm^3)	Substrate	Operating Frequency (GHz)	Bandwidth (GHz)	Gain (dBi)	Application
[6]	35×35×1.6	FR-4	11.55, 12.35, 13.26, 14.23	3.345	5.97, 6.42, 4.97, and 6.05	Wireless communication
[2]	50 × 39 × 0.508	PTFE	0.9, 1.8, 1.9, and 9.2	7.3, 0.9, 1.8	10.8	UWB/ Ground Penetrating Radar (GPR)
[3]	40 × 24.5 × 1.6	FR-4	3.17, 5.82, 7.86, 9.16	8.3	1.7 to 6.25	UWB
[4]	54 ×36 ×1.6	FR-4	2.46, 5, 9.311	9.6	8	UWB/ GPR
[7]	16×13×1.6	FR-4	7.5, 8.5, 12, 13	9.19	1.06, 2.04, 3.91, 4.3	UWB/ GPR
This Work	17×19×0.7	RT/duroid 5880	9.151, 10.234, 16.675	13.62	2.5, 2.96, 3.51	UWB/ GPR/ wireless communication/ radar systems

V. CONCLUSIONS

Relative to the antennas in [6], [7] The proposed design achieves the widest contiguous bandwidth and one of the smallest footprints. With a size of 17×19×0.7 mm^3 (area = 323 mm^2), it is ~74% smaller than [6] (1225 mm^2), ~83% smaller than [2] (1950 mm^2), ~67% smaller than [3] (980 mm^2), and ~84% smaller than [4] (1944 mm^2). Only [7] It is smaller in area (208 mm^2), but our design is ~56% thinner (0.7 mm vs 1.6 mm) and offers substantially broader coverage. In bandwidth, the proposed antenna provides a single UWB window of 13.62 GHz (3.9–17.54 GHz), which is ≈4× wider than [6] (3.345 GHz), ~64% wider than [3] (8.3 GHz), ~42% wider than [4] (9.6 GHz), and ~48% wider than [7] (9.19 GHz); unlike [2], which uses discrete bands, our continuous band simplifies transceiver design and protocol aggregation. Although some references report a higher peak gain as 10.8 dBi in [2] and 8 dBi in [4]. These results come with much larger apertures and/or narrower bands. By contrast, our antenna maintains a practical realized gain of 2.5–3.51 dBi with a linear trend across the band, adequate for short-range, high-throughput UWB links while preserving a very compact form factor. The materials that differentiate the designs from previous designs are FR-4 (higher loss) in most designs and RT/Duroid 5880 for our design, which allows for lower losses and stable dielectric properties, allowing for sustain efficiencies and matching across the broadband UWB. Overall, the proposed antenna provides the best potential for trade-offs between antenna size and contiguous UWB frequency range when compared to [6] and [7], and being capable of multiple domains (UWB/GPR/Wireless/Radar); thus making it suitable for compact multi-standard systems.

The gain values reported for the proposed antenna correspond to realized gain, which accounts for mismatch and radiation losses, including dielectric and conduction effects. In several referenced designs, the reported gain type is not explicitly specified and may represent IEEE gain or peak gain values. This distinction is important, as realized gain provides a more realistic indication of antenna performance under practical operating conditions.To summarize, UWB antennas reported in the literature generally trade off size, bandwidth and gain; some antennas provide high gain but need large apertures, while others are compact but operate with fragmented or narrower bands. On the other hand, the proposed antenna provides a contiguous continuously operating ultra-wideband response from below 6GHz, the X and Ku bands in an extremely small size and low profile, while maintaining consistency in both gain and efficiency for all applications. This combination of size, coverage, and flexibility means that it is uniquely suited to be an excellent solution for future UWB, radar, and multihoping multi-standard wireless applications.

This work presented a novel ultra-compact UWB antenna realized on RT/Duroid 5880 with dimensions of 17 × 19 × 0.7 mm^3. Through a stepwise structural refinement involving ground modification, resonant slots, and loop integration, the antenna achieves a wide contiguous bandwidth of 13.62 GHz (3.9–17.54 GHz), effectively covering Sub-6 GHz, C-, X-, and Ku-bands. This broad spectral span ensures suitability for a wide range of modern applications, including UWB indoor communications, 5G Sub-6 GHz services, Wi-Fi/WiMAX, radar, GPR, cognitive radio, and satellite links.

The novelty of the design lies in its new geometric configuration that combines extreme miniaturization with wideband operation while maintaining stable gain (2.5–3.51 dBi), high efficiency (≈70–80%), and predictable radiation characteristics across the entire operating range. To ensure robustness, the antenna was validated not only in the frequency domain but also in the time domain by integrating CST simulations with MATLAB analysis. The combined evaluation confirmed low distortion, flat group delay, sharp impulse response, and a wide-open eye diagram, thereby demonstrating reliable support for high-data-rate UWB links.

Overall, the proposed antenna offers a compact, fabrication-ready, and versatile solution that balances size, performance, and multi-band functionality, making it well-suited for next-

generation UWB, wireless communication, radar, and sensing platforms.

REFERENCES

[1] Y. Liu, S. Yu, and X. Liu, "A Compact Ultra-Wideband Microstrip Antenna for Spectrum Monitoring," Progress In Electromagnetics Research C, vol. 153, pp. 225–232, 2025, doi: 10.2528/PIERC25011904.

[2] T. Saeidi, A. R. H. Alhawari, A. H. M. Almawgani, T. Alsuwian, M. A. Imran, and Q. Abbasi, "High Gain Compact UWB Antenna for Ground Penetrating Radar Detection and Soil Inspection," Sensors, vol. 22, no. 14, p. 5183, Jul. 2022, doi: 10.3390/s22145183.

[3] I. H. Nejdi et al., "UWB Circular Fractal Antenna with High Gain for Telecommunication Applications," Sensors, vol. 23, no. 8, p. 4172, Apr. 2023, doi: 10.3390/s23084172.

[4] F. ALtalqi, S. Fennane, H. Mabchour, H. Kacimi, and A. Echchelh, "Design monopole antenna of ultra-wideband high bandwidth and high efficiency for ground penetrating radar application," TELKOMNIKA (Telecommunication Computing Electronics and Control), vol. 22, no. 4, p. 812, Aug. 2024, doi: 10.12928/telkomnika.v22i4.25340.

[5] W. Thaiwirot, J. Ardhan, S. Prengsri, P. Akkaraekthalin, and S. Chalermwisutkul, "The low-profile all-textile UWB antenna with AMC for WBAN Applications," EURASIP Journal on Wireless Communications and Networking, vol. 2025, no. 1, p. 56, Jul. 2025, doi: 10.1186/s13638-025-02487-4.

[6] B. V. S. Sailaja and K. K. Naik, "Design of Ultra-Wideband Circular Patch with L-Slits Antenna for Wireless Applications," International Journal of Microwave and Optical Technology, vol. 16, no. 1, 2021.

[7] N. P. S. P. K. S. S. Gupta, "Design and Analysis of Compact CPW-Ultra Wideband Microstrip Patch Antenna for V2X, Sub-6GHz, and other Wireless Applications," Communications on Applied Nonlinear Analysis, vol. 32, Mar. 2025.

[8] D. M. Pozar, Microwave Engineering, 4th ed. Hoboken, NJ, USA: Wiley, 2012.

[9] J. R. James and P. S. Hall, Eds., Handbook of Microstrip Antennas, Volume 1. Institution of Engineering and Technology, 1989. doi: 10.1049/PBEW028F.

[10] L. C. Paul et al., "A compact wrench-shaped patch antenna with a slotted parasitic element and semi-circular ground plane for 5G communication," e-Prime - Advances in Electrical Engineering, Electronics and Energy, vol. 6, p. 100334, Dec. 2023, doi: 10.1016/j.prime.2023.100334.

[11] S. Bhunia, "Effects of Slot Loading on Microstrip Patch Antennas," International Journal of Wired and Wireless Communications, vol. 1, no. 1, 2012.

[12] S. K. Patel, and Y. P. Kosta, "E-shape microstrip patch antenna design for GPS application," in 2011 Nirma University International Conference on Engineering: Current Trends in Technology, NUiCONE 2011 - Conference Proceedings, 2011. doi: 10.1109/NUiConE.2011.6153261.

[13] J. N. Shehab, M. J. Farhan, and S. Al-Azawi, "A non-invasive wearable microwave sensor for Alzheimer's Stage differentiation using realistic 3D human head phantoms," Results in Engineering, vol. 27, p. 106350, Sep. 2025, doi: 10.1016/j.rineng.2025.106350.

[14] J. N. Shehab, M. J. Farhan, and S. Al-Azawi, "Microwave Sensing System and Six-layer Phantom Model for Detection of Benign and Malignant Brain Tumors in Experimental and Simulated Environments," International Journal of Intelligent Engineering and Systems, vol. 18, no. 4, pp. 571–584, May 2025, doi: 10.22266/ijies2025.0531.37.

[15] X. Zhou, J. Le Kernec, and D. Gray, "Vivaldi antenna for railway cutting monitoring," in 2016 CIE International Conference on Radar, RADAR 2016, 2017. doi: 10.1109/RADAR.2016.8059180.

[16] P.-S. Kildal, Foundations of Antenna Engineering: A Unified Approach for Line-of-Sight and Multipath, 1st ed. Artech House, Antennas and Electromagnetics Analysis Library, 2015.

[17] O. Franek and G. F. Pedersen, "Spherical Horn Array for Wideband Propagation Measurements," IEEE Trans Antennas Propag, vol. 59, no. 7, pp. 2654–2660, Jul. 2011, doi: 10.1109/TAP.2011.2152349.

[18] K. Rambabu, A. E. C. Tan, K. K. M. Chan, and M. Y. W. Chia, "Estimation of antenna effect on ultra-wideband pulse shape in transmission and reception," IEEE Trans Electromagn Compat, vol. 51, no. 3 PART 2, 2009, doi: 10.1109/TEMC.2009.2023364.

[19] J. Park, and H. Park, "System-Level Statistical Eye Diagram for Signal Integrity," Electronics (Basel), vol. 13, no. 22, p. 4387, Nov. 2024, doi: 10.3390/electronics13224387.



Jinan N. Shehab received her B.Sc. degree in Electronics Engineering from the University of Diyala, Iraq, and her M.Sc. degree in Electronics and Communications Engineering from Al-Mustansiriyah University, Baghdad. She later obtained her Ph.D. degree in Communications Engineering from Al-Mustansiriyah University in 2025. She is currently a faculty member in the Department of Communications Engineering at the College of Engineering, University of Diyala, where she teaches and supervises undergraduate and graduate research projects. Her research interests include watermarking, steganography, cryptography, UWB antenna design, wearable antennas, and electromagnetic biomedical sensing systems.



Wisam Hayder Mahdi was born in Diyala, Iraq, in 1984. He received the B.Sc. degree in Electronics Engineering from the University of Diyala in Iraq. His M.Sc. degree in MC-CDMA from Erciyes University, Turkey, in 2018, and PhD degree from the same university in "Resource Allocation using intelligent optimization Techniques in device to device (D2D) communication". His main research interests include PAPR reduction in MC-CDMA, Resource Allocation, D2D Communication, 5G, Optimization and wireless Communication. He has been a Lecturer with the University of Diyala, Iraq, since 2020



Israa Hazem Ali received her B.Sc degree in Electronics Engineering from the University of Diyala, Iraq, and her M.Sc. degree in Electronics and Communications Engineering from Al-Mustansiriyah University, Baghdad. She is currently a faculty member in the Department of Communications Engineering at the College of Engineering, University of Diyala, where she teaches and supervises undergraduate and graduate research projects. Her research interests include microwave antenna, biomedical antenna, fractal and metamaterial antenna, MIMO and drone antenna.